Investigation on the reactivity of dithiophosphonato/dithiophosphato Ni^{II} complexes towards 2,4,6-tris-2-pyridyl-1,3,5-triazine: developments and new perspectives†

M. Carla Aragoni,*[a] Massimiliano Arca,[a] Miriam Crespo,[a] Francesco A. Devillanova,[a] Michael B. Hursthouse,[b] Susanne L. Huth,[b] Francesco Isaia,[a] Vito Lippolis[a] and Gaetano Verani[a]

Received 30th October 2008, Accepted 16th December 2008
First published as an Advance Article on the web 17th February 2009
DOI: 10.1039/b819326f

The reactions between tptz and differently substituted dithiophosphonato $[Ni(ROpdt)_2]$ [ROpdt = $(RO)(4\text{-}MeOC_6H_4)PS_2^-$; R = Et (**2**); Pr (**3**); *i*-Pr (**4**); Bu (**5**)] and dithiophosphato $[Ni((EtO)_2PS_2)_2]$ (**6**) Ni^{II} complexes have been investigated, and the characterisation of the resulting neutral mixed complexes (**2**·tptz)-(**6**·tptz) is reported. In all these complexes, tptz forces one of the two dithiophosphonato/dithiophosphato ligands to behave as a monodentate ligand, a coordination mode rarely found in analogous Ni^{II} phosphorodithioato complexes. A comparison has been performed between the Ni–S bond distances of the new complexes and those of isologous dithiophosphonato, dithiophosphato and dithiophosphito Ni^{II} square-planar complexes, and of their penta- and hexa-coordinated adducts. The results, also supported by DFT calculations, are discussed and explained in terms of the structural *trans*-effect (STE). The reactivity of **2**·tptz towards $AgNO_3$ and $CuSO_4$ to yield the complex $[Ni(EtOpdt)(tptz)(H_2O)]NO_3$ (**7**), and the dimer $[(Ni(tptz)(\mu\text{-}SO_4)(H_2O)]_2\cdot 6H_2O$ (**8**), respectively, is consistent with the proposed bonding models.

Introduction

The preparation of coordination polymers by the self assembly of neutral metal complexes and donor molecules *via* coordination bonds or secondary bonding interactions is of increasing importance in the field of crystal engineering.[1] In this context, we have started a synthetic program based on the ability of neutral dithiophosphonato Ni^{II} complexes $[Ni(ROpdt)_2]$ [ROpdt = $(RO)(4\text{-}MeOC_6H_4)PS_2^-$; R = alkyl substituent][2] to act as building blocks for the predictable assembly of inorganic coordination polymers. Due to its coordinative unsaturation, the Ni^{II} ion in these square-planar complexes tends to complete its coordination sphere through axial binding of monodentate donor molecules, such as pyridine, to yield octahedral complexes.[3,4] Therefore, by using suitable N-L-N bidentate bipyridyl-based spacers, we prepared 1D coordination polymers of the type $[Ni(ROpdt)_2(N\text{-}L\text{-}N)]_\infty$.[5,6] The primary structural motif of the polymers has proved to depend mainly on the features of the pyridyl-based spacers such as length, rigidity, number and orientation of the donor atoms, whereas the –OR substituents on the phosphorus atoms influence the final 3D-architecture through hydrogen bonds and face-to-face or edge-to-face π–π interactions.[5] Recently,[7] we explored the reactivity of the dithiophosphonato Ni^{II} complex $[Ni(MeOpdt)_2]$ (**1**) towards 2,4,6-tris-2-pyridyl-1,3,5-triazine (tptz; Chart), which belongs to the class of *multi-modal* ligands,[8] since it contains both chelating and monodentate donor sites, and is of current interest in the design of multinuclear metal complexes.[9] However, our plan to use the multimodal tptz to build multidimensional networks was not achieved since tptz behaved as a tridentate ligand rather than achieving higher denticity, and we obtained an unusual mixed tptz-dithiophosphonato complex $[Ni(MeOpdt)_2(tptz)]$ (**1**·tptz). In this, the non-coordinating sites are available to interact with suitable Lewis acids, exemplified by the preparation of some interesting products on reaction with I_2 and Br_2.[7] We have now extended our investigations on the mixed complexes obtained by reacting tptz with differently substituted dithiophosphonato $[Ni(ROpdt)_2]$ [R = Et (**2**), Pr (**3**), *i*-Pr (**4**), Bu (**5**)] and dithiophosphato $[Ni((EtO)_2PS_2)_2]$ (**6**) complexes (Chart 1).

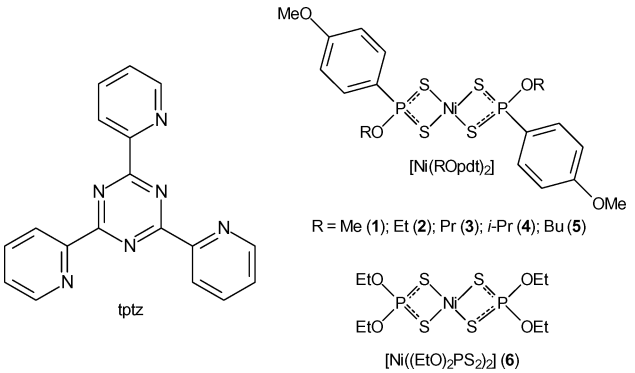

Chart 1

[a]*Dipartimento di Chimica Inorganica ed Analitica, Università degli Studi di Cagliari, S.S. 554 bivio per Sestu, 09042, Monserrato-Cagliari, Italy. E-mail: aragoni@unica.it; Fax: +39 070 6754456; Tel: +39 070 6754491*
[b]*School of Chemistry, University of Southampton, Highfield, Southampton, UK SO17 1BJ*

† Electronic supplementary information (ESI) available: Selected hydrogen bond distances (Å) and angles (°) for compounds **2**·tptz, **3**·tptz, **4**·tptz, **6**·tptz, **7**, and **8** are reported in Table S1. Molecular view of compound **6**·tptz is reported in Figure S1. Packing views of compounds **2**·tptz, **4**·tptz, **7**, and **8** are reported in Figures S2, S3, S4, and S5, respectively. CCDC reference numbers 278292–707537. For ESI and crystallographic data in CIF or other electronic format see DOI: 10.1039/b819326f

Results and discussion

The reactions of the dithiophosphonato complexes [Ni(ROpdt)$_2$] [ROpdt = (RO)(4-MeOC$_6$H$_4$)PS$_2^-$; R = Et (**2**); Pr (**3**); *i*-Pr (**4**); Bu (**5**)] and tptz in 1 : 1 molar ratio in the corresponding ROH alcohols, yielded crystals of the complexes [Ni(ROpdt)$_2$tptz] [R = Et (**2**·tptz); Pr (**3**·tptz); *i*-Pr (**4**·tptz); Bu (**5**·tptz)]. Similarly, the reaction in EtOH of the dithiophosphato complex [Ni((EtO)$_2$PS$_2$)$_2$] (**6**) and tptz in 1 : 1 molar ratio, afforded compound [Ni((EtO)$_2$PS$_2$)$_2$tptz] (**6**·tptz). Single crystal X-ray diffraction has been performed on all compounds; crystallographic data and selected bond lengths and angles for **2**·tptz, **3**·tptz, **4**·tptz, **5**·tptz, and **6**·tptz are reported in Tables 1 and 2, respectively.[10] As exemplified in Fig. 1 for the case of **2**·tptz, in all compounds **2**·tpz-**6**·tpz, a molecule of tptz coordinates the nickel ion imposing an expansion and rearrangement of the metal coordination sphere from square planar to distorted octahedral. The Ni^{II} ion is thus coordinated by the three nitrogen atoms N1, N4, and N5 from tptz and three sulfur atoms belonging to a bidentate (S1 and S2) and a monodentate (S3) dithiophosphonato ligand, respectively, arranged in a meridian fashion. The formation of five-membered chelate rings with small rigid N–Ni–N bites [N–Ni–N *av.* 77.0 Å] is reflected in the geometry around the nickel, with N–Ni–S angles diverging from the ideal values of 90 and 180° (Table 2). The bond distances Ni–N1 between the Ni ion and the triazine nitrogen atoms range from 1.968(2) to 1.990(6) Å and are significantly shorter than the other Ni–N4 and Ni–N5 distances [*av.* 2.141 and 2.125 Å, respectively], analogous to what was found in the case of [Ni(MeOpdt)$_2$tptz] (**1**·tptz)[7] and other nickel complexes with tptz.[20,21]

As evidenced by a Mogul geometry check,[11] in compounds **1**·tptz–**6**·tptz the octahedral Ni^{II} coordination cores present unusual Ni–S bond distances: the dithiophosphonato/dithiophosphato chelating moieties behave as strongly anisobidentate ligands and feature one short and one long Ni–S distance (Ni–S1, av. 2.40; Ni–S2, av. 2.57 Å, see Table 2). By searching the Cambridge Structural Database (CSD) for appropriate data, we compared the Ni–S distances in the bidentate fragments of compounds **1**·tptz–**6**·tptz with those of dithiophosphonato fragments behaving as bidentate ligands belonging to square-planar nickel(II) complexes or to their octahedral complexes with both monodentate and bidentate pyridine based ligands (Fig. 2).[12] The examination of the data confirms that both Ni–S1 and Ni–S2 bond distances are quite unusual, notwithstanding their average values falling in the range expected for fragments belonging to octahedral complexes. In fact, the short Ni–S1 bond distances (around 2.4 Å, grey full bars in Fig. 2) fall in a range of values intermediate between those observed in square planar dithiophosphonato complexes (around 2.2 Å, dashed bars in Fig. 2) and those reported for the octahedral adducts (around 2.5 Å, empty bars, Fig. 2), whilst the Ni–S2 bond distances (around 2.6 Å, black full bars in Fig. 2) are somewhat longer than those commonly observed. Similar but less pronounced elongations of one of the two Ni–S bonds have been found in analogous dithiophosphato bidentate fragments belonging to *cis*-octahedral adducts between dithiophosphato nickel(II) complexes and pyridine based donors, and explained in terms of the structural *trans*-effect (STE)[13] of the nitrogen donors.[14] We have thus extended the structural comparison by plotting Ni–S1 *vs.* Ni–S2 bond distances of the

Table 1 Crystal data collections and refinements for compounds **2**·tptz–**6**·tptz, **7**, and **8**[10]

	2·tptz	**3**·tptz	**4**·tptz	**5**·tptz	**6**·tptz	**7**	**8**
Empirical formula	$C_{36}H_{36}N_6NiO_4P_2S_4$	$C_{38}H_{40}N_6NiO_4P_2S_4$	$C_{38}H_{40}N_6NiO_4P_2S_4$	$C_{40}H_{44}N_6NiO_4P_2S_4$	$C_{26}H_{32}N_6NiO_4P_2S_4$	$C_{27}H_{28}N_6NiO_3PS_2{\cdot}NO_3$	$C_{36}H_{28}N_{12}Ni_2O_{10}S_6(H_2O)$
M	865.62	893.67	893.67	921.72	741.49	698.35	1078.32
Crystal system	Triclinic	Triclinic	Orthorhombic	Monoclinic	Monoclinic	Triclinic	Triclinic
Space group	*P*-1 (no. 2)	*P*-1 (no. 2)	*Pbca* (no. 61)	*P2(1)/c* (no. 14)	*P2(1)/c* (no. 14)	*P*-1 (no. 2)	*P*-1 (no. 2)
a (Å)	11.3304(3)	12.5691(7)	12.0483(15)	16.294(2)	8.770(2)	10.578(3)	8.5672(11)
b (Å)	13.1931(3)	13.3601(7)	25.569(3)	20.6419(18)	13.0216(19)	11.808(4)	11.0578(15)
c (Å)	14.5372(2)	13.8241(7)	26.479(2)	12.5615(10)	29.654(8)	13.972(7)	11.8063(14)
α (°)	105.484(1)	76.563(2)	90	90	90	113.89(4)	71.926(6)
β (°)	101.243(1)	81.865(2)	90	91.260(8)	93.64(2)	104.80(3)	77.024(7)
γ (°)	98.871(1)	72.466(3)	90	90	90	96.21(2)	77.929(7)
Volume (Å^3)	2004.50(8)	2146.5(2)	8157.2(15)	4223.9(7)	3379.6(13)	1497.9(12)	1024.3(2)
Z	2	2	8	4	4	2	1
D_{calc} (Mg/m^3)	1.434	1.383	1.455	1.449	1.457	1.548	1.748
μ (mm^{-1})	0.818	0.767	0.807	0.782	0.957	0.895	1.113
θ min-max (°)	3.0–27.5	3.2–25.0	3.0–21.8	3.1–27.5	2.9–27.5	3.0–25.0	3.0–27.5
Refl.Collected/unique	40210/9162	65715/7530	39380/4411	32213/9665	27618/7649	26049/5259	16334/3584
Refl.obs.($I > 2\sigma I$)	7171	4862	2772	6694	5272	3160	2495
R/R_{INT}	0.0489/0.039	0.1124/0.167	0.0666/0.164	0.0904/0.065	0.0522/0.070	0.0631/0.25	0.0867/0.165
wR2	0.1388	0.2110	0.1527	0.1880	0.1618	0.1497	0.1456

Table 2 Selected bond lengths (Å) and angles (°) for compounds **2**·tptz–**6**·tptz, and **7**. Values for **1**·tptz[7] are reported for completeness

	1·tptz	**2**·tptz	**3**·tptz	**4**·tptz	**5**·tptz	**6**·tptz	**7**
Ni–N1	1.965(3)	1.968(2)	1.990(6)	1.976(7)	1.987(4)	1.970(3)	1.981(5)
Ni–N4	2.170(3)	2.135(2)	2.135(7)	2.143(8)	2.153(5)	2.139(3)	2.169(5)
Ni–N5	2.141(3)	2.125(2)	2.118(7)	2.106(6)	2.147(5)	2.130(3)	2.147(6)
Ni–S1	2.384(1)	2.4005(9)	2.419(2)	2.402(3)	2.411(2)	2.4220(12)	2.403(2)
Ni–S2	2.569(1)	2.6045(9)	2.569(2)	2.558(3)	2.5470(19)	2.5603(12)	2.501(2)
Ni–S3/O3	2.459(1)	2.4130(9)	2.421(2)	2.437(2)	2.4369(17)	2.4242(12)	2.067(4)
P1-S1	2.002(1)	1.9992(13)	2.005(3)	2.008(3)	1.983(3)	1.9784(14)	2.009(2)
P1-S2	1.994(1)	1.9864(13)	1.988(3)	1.982(3)	1.969(3)	1.9919(14)	1.986(2)
P2-S3	2.009 (1)	2.0254(10)	2.011(3)	2.020(3)	2.010(2)	1.9920(14)	—
P2-S4	1.960(1)	1.9579(10)	1.970(3)	1.942(3)	1.965(2)	1.9553(16)	—
N1-Ni–S1	174.24(9)	169.24(7)	168.3(2)	172.52(19)	171.73(14)	173.04(9)	178.57(15)
N1-Ni–S2	92.54(9)	87.15(7)	87.12(19)	90.74(18)	90.70(13)	91.74(9)	85.82(15)
N1-Ni–S3/O3	96.38(9)	103.37(7)	105.3(2)	100.18(18)	102.61(13)	98.19(9)	88.71(18)
N1-Ni–N5	76.8(1)	77.40(9)	77.1(3)	77.3(3)	77.0(17)	77.28(13)	76.9(2)
N4-Ni–N5	153.6(1)	154.06(9)	153.5(3)	154.2(3)	153.32(19)	154.07(11)	153.11(18)
N4-Ni–S1	102.35(9)	102.61(7)	102.54(19)	100.6(2)	102.87(15)	100.70(8)	104.33(13)
N4-Ni–N1	76.8(1)	76.71(9)	76.4(3)	77.1(3)	76.31(17)	76.97(13)	76.3(2)
N5-Ni–S1	104.02(9)	103.11(7)	103.32(19)	104.2(2)	103.56(15)	105.23(8)	102.48(15)
S1-Ni–S2	81.78(4)	82.11(3)	81.23(7)	82.00(8)	81.04(7)	81.72(4)	82.93(7)
S1-P1-S2	108.63(7)	111.30(5)	108.92(13)	109.39(14)	109.30(12)	110.45(6)	108.79(11)
S3-P2-S4	116.58(7)	117.81(4)	113.46(13)	120.49(15)	118.23(10)	114.33(7)	—

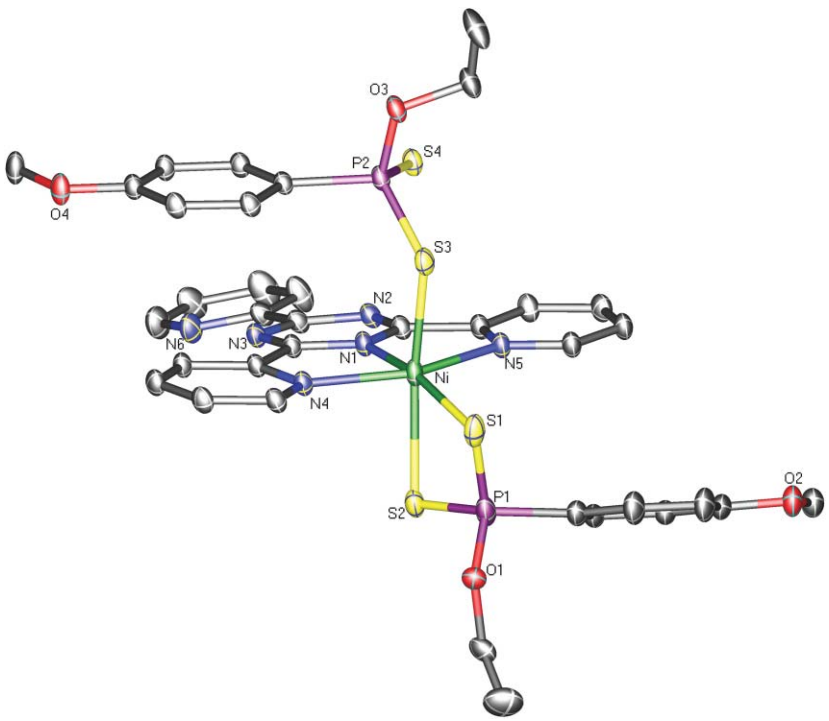

Fig. 1 Molecular view of compound **2**·tptz. For clarity, only non-carbon atoms have been labelled and hydrogen atoms omitted. Displacement ellipsoids are drawn at 50% probability level.

title compounds and of analogous bidentate dithiophosphonato [$(R'(RO)PS_2)^-$, circles in Fig. 3], dithiophosphato [$((RO)_2PS_2)^-$, triangles in Fig. 3], and dithiophosphito [$(R_2PS_2)^-$, squares in Fig. 3] fragments bound to nickel(II) ions present in the CSD; the results are summarized in Fig. 3.[15] Three main regions can be recognized, as not depending on the nature of the P-substituents, which represent complexes with analogous coordination geometries: square-planar complexes (blue), octahedral (green) and square-pyramidal penta-coordinate (red squares) adducts. It is interesting to note that both octahedral adducts with configuration *trans* and *cis* (empty and filled green markers, respectively) are clustered in the same area, which shows a significant spread. This is in agreement with a certain asymmetry found within the PS_2Ni fragments belonging to several octahedral adducts, in particular those featuring a *cis* configuration, resulting from a STE of the nitrogen donors.[14] On the contrary, the Ni–S bond distances in (**1**·tptz)-(**6**·tptz) (black circles) do not fall in the expected region of octahedral complexes, but define a separate area. Only

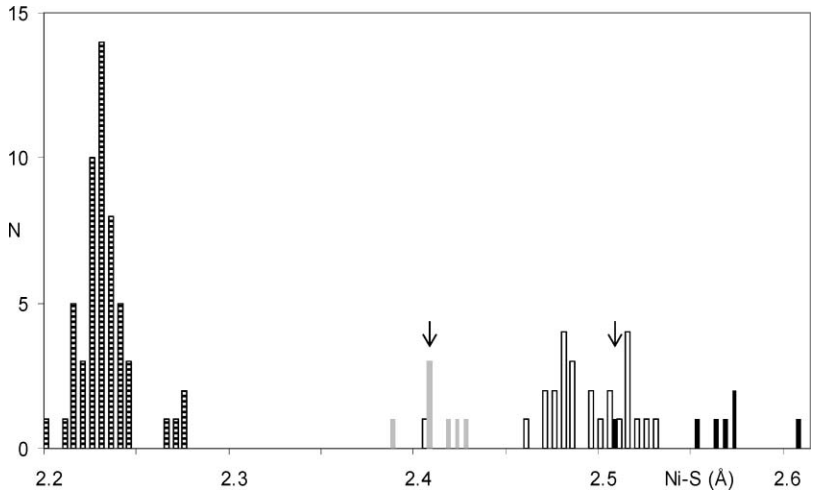

Fig. 2 Histograms for the Ni–S bond lengths within dithiophosphonates behaving as bidentate ligands in Ni^{II} complexes; dashed bars: square planar complexes;[12] empty bars: octahedral complexes;[12] full bars: compounds **1**·tptz–**6**·tptz (grey, Ni–S1; black: Ni–S2); arrows on full bars point out compound **7**.

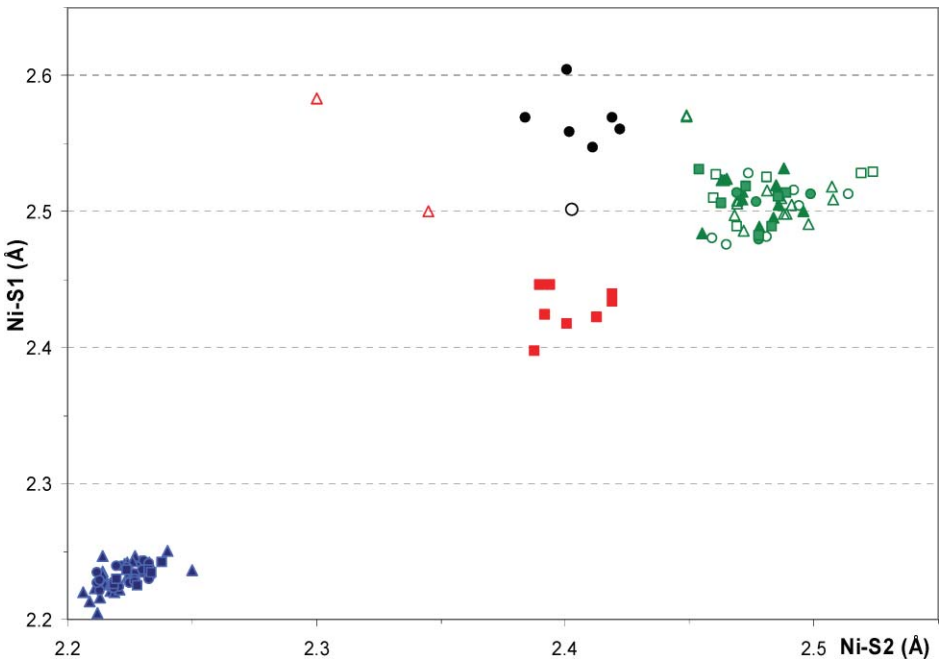

Fig. 3 Scatter plot of Ni–S1 *vs.* Ni–S2 bond lengths for the bidentate dithiophosphonato [$(R(RO)PS_2)^-$, circles], dithiophosphato [$((RO)_2PS_2)^-$, triangles], and dithiophosphito [$(R_2PS_2)^-$, squares] fragments bound to nickel(II) ions.[15] Different colours refer to different coordination geometries: square-planar (blue); octahedral (green: *cis* and *trans* configurations are evidenced by using full and empty symbols, respectively); penta-coordinated (red: *square pyramidal* and *trigonal bipyramidal* geometries are evidenced by using full and empty symbols, respectively); compounds **1**·tptz–**6**·tptz full black; compound **7** empty black.

two compounds, among the 105 analyzed, present Ni–S bond lengths falling out of the three main regions, and both feature a dithiophosphato moiety behaving as monodentate ligand *trans* to the longer Ni–S distance (red triangles). Notwithstanding the lack of comparable fragments providing more confidence, it can be deduced that monodentate dithiophosphonato/dithiophosphato ligands exercise a notable STE which causes a stretching of the *trans* disposed Ni–S bonds, and a shortening of the corresponding *cis* Ni–S bonds. This can be explained from a classical point of view by using the Grinberg polarisation theory,[16] which attributes the weakening of the bond of a certain ligand to the presence of an easily polarisable donor group [in our case the $P(=S)S^-$ fragment] *trans* disposed with respect to the ligand itself, since it causes an increase of negative charge on the metal and consequently a partial repulsion of the ligand. This classical description of the STE was rationalized in more recent years by Burdett and Albright in terms of MO analyses of octahedral complexes,[17] demonstrating that if two different ligands are forced to share the same metal atomic orbital a differential weakening of the metal–ligand bonds occurs.

In the second dithiophosphonato/dithiophosphato unit, which behaves as monodentate ligand, the Ni–S3 bond distance is only slightly elongated with respect to those observed in square-planar dithiophosphonato Ni^{II} complexes, and the two P–S bond distances are quite different since the one not involved in the metal–sulfur bond (P2–S4) retains a double bond character. Tptz is only roughly planar with the pyridyl rings unequally twisted with respect to the central triazine ring due to intermolecular H-bonds and π-interactions which control the crystal packing. Notwithstanding the structure of complexes **2**·tptz–**6**·tptz closely resemble each other, the corresponding crystal packing are different, mainly depending on the nature of the P-substituents. The presence of aromatic P-substituents leads the molecules to pack driven by aromatic interactions. Thus, compounds **2**·tptz, **3**·tptz, and **5**·tptz, featuring an anisole and linear alkyl chains of different length as the P-substituents, pack in pairs, disposed around an inversion centre, interacting through either off-set or slipped face-to-face π–π interactions between the aromatic rings of tptz and anisole moiety to form layered piles or sheets (Fig. 4, and Fig. S2 in ESI†). The OR chains protrude to join adjacent piles or sheets through interactions of the type X···H (X = S and O; Fig. S2 and S3b in ESI†). In contrast, in the case of compound **4**·tptz, the complex molecules do not pair off, but pack piled along the direction of the *c* axis, positioned in order to enhance π–π interactions between adjacent piles (Fig. S3 in ESI†).

Also in the case of **6**·tptz, which features two OEt P-substituents, aromatic interactions show their importance in organizing the packing by ordering molecules of **6**·tptz in pairs by means of a perfect off-set π–π interaction between the two $C_5N(4)$ pyridine rings of symmetry related tptz molecules (parallel planes at 3.49 Å). In contrast to what was observed in the previously discussed structures, these interactions are isolated to the two involved rings, the packing of the paired molecules being left to C–H···S interactions between the sulfur atoms and the OEt P-substituents and the tptz $C_5N(4)$ pyridine rings (Fig. 5).

DFT calculations

With the aim of a better understanding of the nature of the bonding in the mixed tptz-dithiophosphonato/dithiophosphato Ni^{II} complexes DFT calculations have been performed on the compounds **2**·tptz and **6**·tptz. The electronic structures of the two complexes show that they present similar features although some differences in the relative energy order of the frontier Kohn–Sham orbitals can be found due to the contribution of the orbitals of the aromatic P-substituents in **2**·tptz. In particular, it is worth observing that both **2**·tptz and **6**·tptz feature filled bonding molecular orbitals involving the interaction of the d atomic orbitals of the central nickel ion with those localized on the lone pairs of the sulfur atoms (S2 and S3) *trans* disposed to each other (Fig. 6). This is in agreement with the structural *trans*-effect (STE) evidenced on the ground of structural data discussed above. Moreover, on the basis of recent work by Arden and Orpen,[18] which analyzes the STE in terms of the involved molecular orbitals, for M–L bonds having a substantial d_{Ni}-orbital character a certain *trans*-influence[13] accompanied by a less important *cis*-influence is expected, in agreement with that discussed above. More detailed information on the nature of the bonding between the central metal ion and the ligands in complexes **2**·tptz and **6**·tptz come from a natural bond orbital analysis. Natural charges, calculated on the metal centre and on the S and N donor atoms are summarized in Table 3. In both cases, as expected, sulfur atoms coordinating the nickel centre are more negatively charged than nitrogen ones. Interestingly, in compound **2**·tptz, the central ion is more positively charged than in **6**·tptz, while the corresponding donor atoms are more negatively charged, indicating a decrease in the polarization

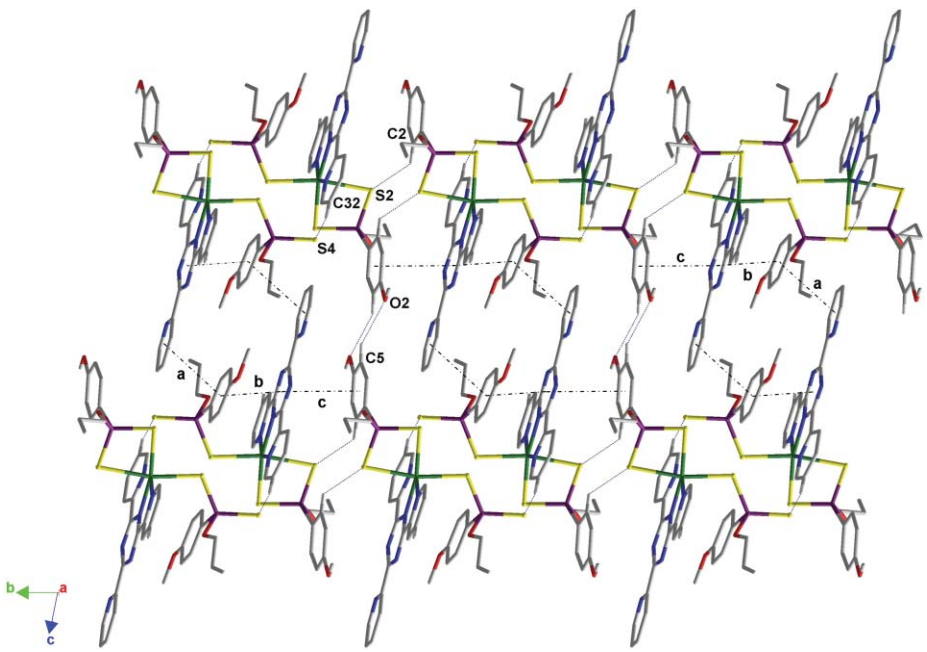

Fig. 4 Packing view of compound **3**·tptz evidencing H-bonds and π–π interactions between the aromatic rings of tptz and anisole to form layered sheets [C2–H2···S2: 2.84, 3.478(8), 125.0; C32–H32···S4: 2.72, 3.581(10), 151.0; C5–H5···O2: 2.43 Å, 3.312(11) Å, 154.0°; **a**: 3.71, 7.26; **b**: 3.93, 5.52; c: 3.75 Å, 11.4°]. Hydrogen atoms not involved in the interactions shown have been omitted for clarity reasons.

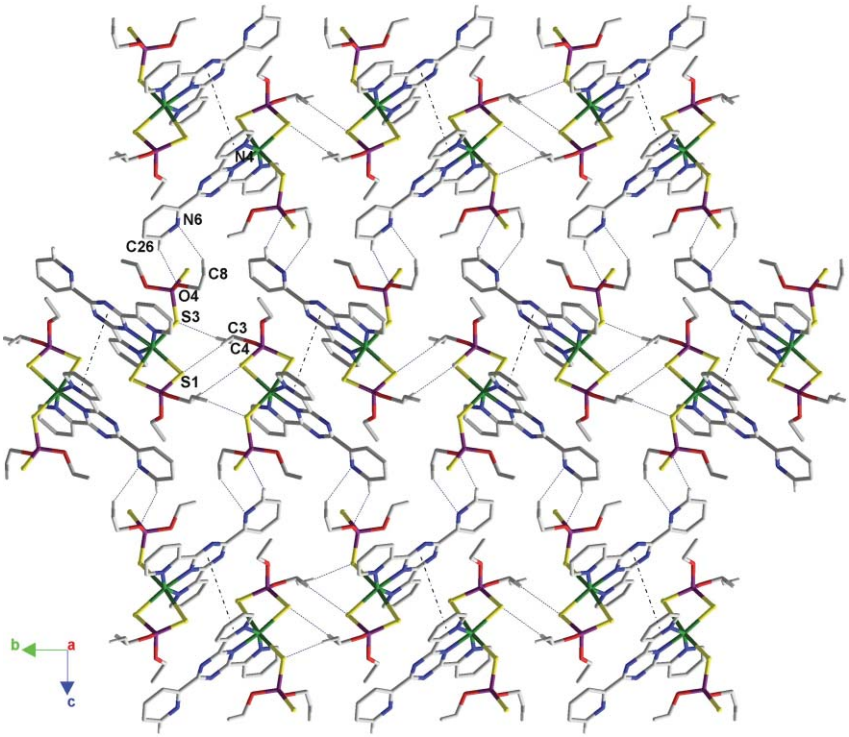

Fig. 5 Packing view of compound **6**·tptz evidencing H-bonds and contacts between π–π paired molecules in the *bc* plane. [$C_3N_3 \cdots C_5N(4)$ 0°, 3.49 Å; C4–H4b $\cdots$ S3: 2.84 Å, 3.632(5) Å, 138°; O4 $\cdots$ H26 2.67; N6 $\cdots$ H8c 2.67; S1 $\cdots$ H3B 3.05 Å] Hydrogen atoms not involved in the interactions shown have been omitted for clarity reasons.

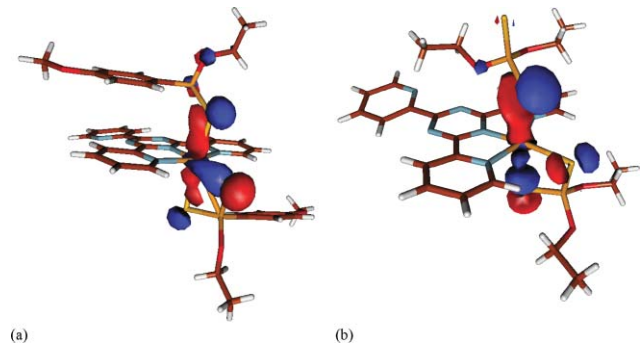

Fig. 6 Drawings of the filled Kohn–Sham molecular orbitals [HOMO-12, (a); HOMO-5, (b)] showing the same d nickel atomic orbital shared between the two axially bonded dithiophosphonato/dithiophosphato ligands in complexes (**2**·tptz, a) and (**6**·tptz, b). Contour value = 0.05 e.

Table 3 Selected NBO charges (e) calculated for **2**·tptz and **6**·tptz at DFT level.[a,b]

	2·tptz	**6**·tptz
Ni	1.157	1.138
P1	1.433	1.676
P2	1.421	1.642
S1	–0.580	–0.612
S2	–0.646	–0.627
S3	–0.695	–0.658
S4	–0.685	–0.650
N1	–0.591	–0.585
N4	–0.542	–0.541
N5	–0.542	–0.537

[a] mPW1PW functional; Shafer, Horn, and Ahlrichs pVDZ basis set. [b] Numbering scheme refers to Fig. 1, and is consistent with all the structures reported.

of the bonds involving the metal when dithiophosphonato anions are replaced by dithiophosphato ones. An examination of the charge distribution on the tptz ligand shows that in both cases the nitrogen donor atom belonging to the triazine ring (N1) is more negatively charged than those (N4 and N5), more distant from the nickel ion, belonging to the coordinating pyridine pendants. Accordingly, Wiberg bond indexes (WBIs)[28] between the metal ion and N1 are remarkably higher than those involving N4 and N5 (Table 4). WBIs also allow for a comparison between the bond feature of monodentate and bidentate dithiophosphonato and dithiophosphato ligands, in **2**·tptz and **6**·tptz, respectively. In both cases, it is worth noting that the two axial sulfur donor atoms S2 and S3 are bonded to the central ion with different strengths: indeed in all cases the sulfur atom belonging to the monodentate ligand (S3) features a more negative charge and coordinates more strongly the nickel as compared to the *trans*-disposed sulfur atom S2, belonging to the bidentate unit. This accounts for the STE exerted by the monodentate unit, in agreement with the theories of Grinberg[16] and Burdett.[17] In contrast, the second sulfur atom of the bidentate unit (S1), is free to strongly bind the nickel ion, and accordingly it shows the higher Ni–S bond order. A further insight into the electronic structures of complexes **2**·tptz and **6**·tptz arises from the analysis of the second order perturbation of the Fock matrix in NBO basis. As regards the tptz ligand, this approach confirms the more coordinating

Table 4 Selected Wiberg bond indexes calculated for **2**·tptz and **6**·tptz at DFT level[a,b]

	2·tptz	**6**·tptz
Ni–S1	0.447	0.404
Ni–S2	0.187	0.242
Ni–S3	0.245	0.293
Ni–S4	0.007	0.035
Ni–N1	0.290	0.284
Ni–N4	0.133	0.118
Ni–N5	0.137	0.109

[a] mPW1PW functional; Shafer, Horn, and Ahlrichs pVDZ basis set. [b] Numbering scheme refers to Fig. 1, and is consistent with all the structures reported.

nature of N1, whose lone pair interaction with the d-type natural bond orbitals localized on the nickel ion amounts to 58.7 and 56.5 Kcal/mol for **2**·tptz and **6**·tptz, respectively, compared to average values of 30.05 and 28.11 Kcal/mol calculated for N4 and N5, in compounds **2**·tptz and **6**·tptz, respectively. As regards the coordinating dithiophosphonato/dithiophosphato ligands, three types of interactions between two lone pairs localized on the sulfur atoms and the empty d-NBOs on the nickel centre have been calculated for both complexes. An examination of the trend of the energies involved allows quantification of the STE described before, which is expected to be more evident in the case of **2**·tptz as compared to **6**·tptz, as experimentally found (Table 2). In fact, the S3 atoms of the monodentate units interact with the nickel ion with energies of 68.17 and 75.79 Kcal/mol, for **2**·tptz and **6**·tptz, respectively, while the *trans* disposed S2 atoms show a remarkably lower interaction energy of 38.16 and 52.81 Kcal/mol, for **2**·tptz and **6**·tptz, respectively. Again, the S1 donor atoms, with no S atoms in the *trans* position, feature the highest energy (105.31 and 90.36 Kcal/mol, for **2**·tptz and **6**·tptz, respectively).

Reactivity

A common feature of complexes (**1**·tptz)–(**6**·tptz) is the presence of donor atoms (N2, N3, N6, and S4, Fig. 1) potentially available to interact with suitable Lewis acids. However, when **2**·tptz was made to react with $AgNO_3$ and $CuSO_4$ we experienced the partial or complete expulsion of the dithiophosphonato ligands from the Ni^{II} coordination sphere, obtaining the complex $[Ni(EtOpdt)(tptz)(H_2O)]NO_3$ (**7**), and the dimer $[(Ni(tptz)(\mu\text{-}SO_4)(H_2O)]_2\cdot 6H_2O$ (**8**), respectively. Single crystal X-ray analysis of **7** reveals that the cationic complex $[Ni(EtOpdt)(tptz)(H_2O)]^+$ presents a coordination environment similar to that of the starting $[Ni(EtOpdt)_2(tptz)]$ (**2**·tptz) with one water molecule in place of one of the two dithiophosphonato ligands EtOpdt originally present. A nitrate anion counterbalances the positive charge. Crystal data and selected bond lengths and angles for **7** are reported in Tables 1 and 2; Fig. 7 shows the complex unit, along with the atom labeling scheme. Nickel–nitrogen bond distances and angles are comparable to those found for complexes **2**·tptz; the Ni–O distance [2.067(4) Å] is similar to that normally found in nickel(II)–aquo complexes.[19] The dithiophosphonato ligand shows similar P–S bond lengths, compatible with a delocalization of the negative charge on the whole fragment. In contrast, the Ni–S bond distances differ slightly from each other, with values falling outside the Ni–S bond-regions previously described

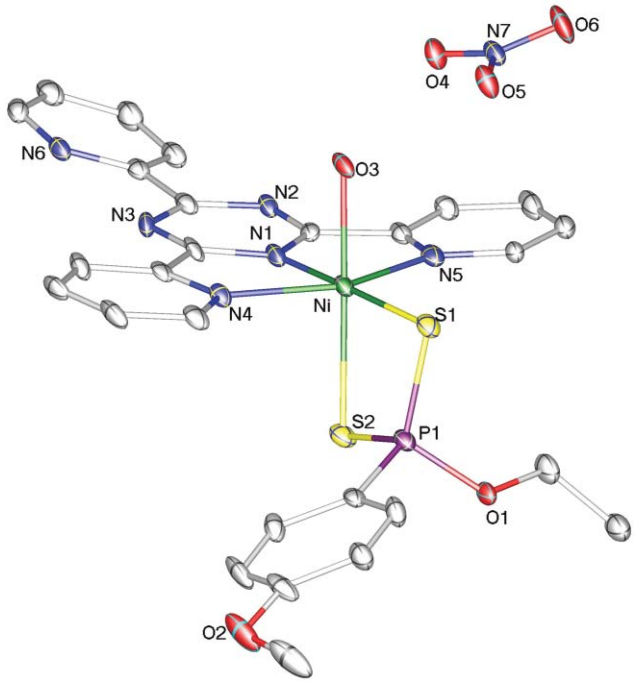

Fig. 7 Molecular view of compound **7**. For clarity, only non-carbon atoms have been labelled and hydrogen atoms omitted. Displacement ellipsoids are drawn at 50% probability.

[Ni–S1, 2.403(2); Ni–S2, 2.501(2) Å; arrows on full bars in Fig. 2, empty black circle in Fig. 3]. The N–O distances in the nitrate anion are quite similar, as expected when the negative charge is delocalized over the whole anion. In contrast to what was observed in the previous compounds, the tptz moiety shows less planarity, with the three pyridyl rings being angled at 3.3, 8.4, and 14.3° with respect to the plane of the central triazine, due to packing effects. In fact, due to the intrinsic differences between the two compounds, the packing of **7** is quite different from that of **2**·tptz, and features planes of parallel ribbons built up by π–π interactions between symmetry related moieties and a dense hydrogen-bonding network involving the apical water molecules, the nitrate anions, and the cationic complex (Fig. S4 in ESI†).

The single crystal X-ray analysis of **8** shows a dimeric structure where two Ni(tptz) units are bridged about a centre of symmetry by two bidentate sulfate anions. Table 1 contains the crystal data for **8**·$6H_2O$ and Fig. 8 shows the dimeric unit, along with the atom labeling scheme. The dithiophosphonato ligands have been completely detached and each Ni^{II} ion displays a distorted octahedral environment where three nitrogen atoms from tptz and an oxygen atom (O4) from one sulfate anion define the equatorial plane of the octahedron; one oxygen atom from the symmetry related sulfate anion and one from a water molecule (O4 and O5, respectively) occupy the axial positions. Nickel–nitrogen bond distances and angles are comparable to those found for complexes **1**·tptz–**6**·tptz, and for other complexes containing a Ni(tptz) moiety.[20,21] The S–O distances in the sulfate anions are similar, thus suggesting a delocalization of the negative charge over the whole anion. The triazine and the two pyridyl rings of tptz bound to the central ion show a good planarity, while the terminal pyridyl ring deviates from planarity, being angled at 19° with respect to the central triazine plane, due to a strong

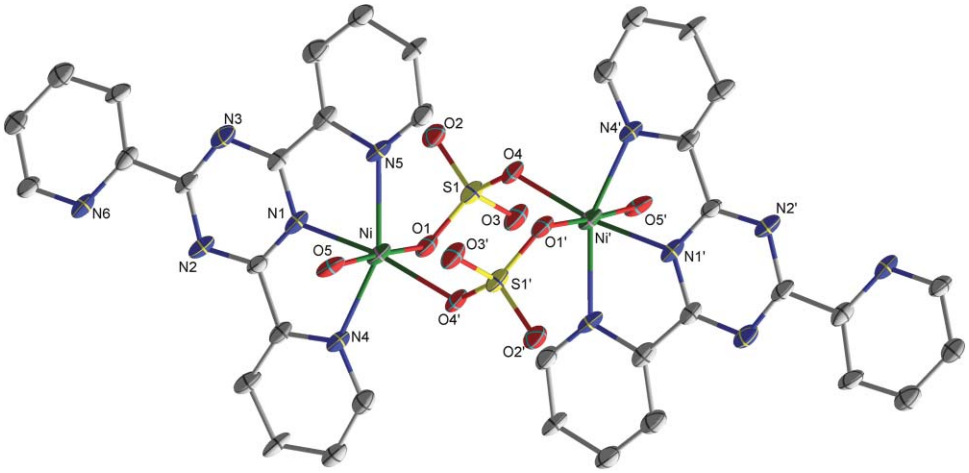

Fig. 8 Molecular view of compound **8**. For clarity, only non-carbon atoms have been labelled and hydrogen atoms and solvent water molecules omitted. Displacement ellipsoids are drawn at 50% probability. Selected bond lengths and angles: Ni–N1, 1.978(6); Ni–N4, 2.127(6); Ni–N5, 2.152(6); Ni–O1, 2.063(5); Ni–O4′, 2.002(5); Ni–O5, 2.123(5); S1-O1, 1.483(5); S1-O2, 1.476(5); S1-O3, 1.478(5); S1-O4, 1.496(5) Å; N1-Ni–N4, 77.2(2); N1-Ni–N5, 76.7(2); O1-Ni–O5, 177.4(2); O1-Ni–N1, 90.2(2)°. Symmetry codes: ′ –x, –y, 2 – z.

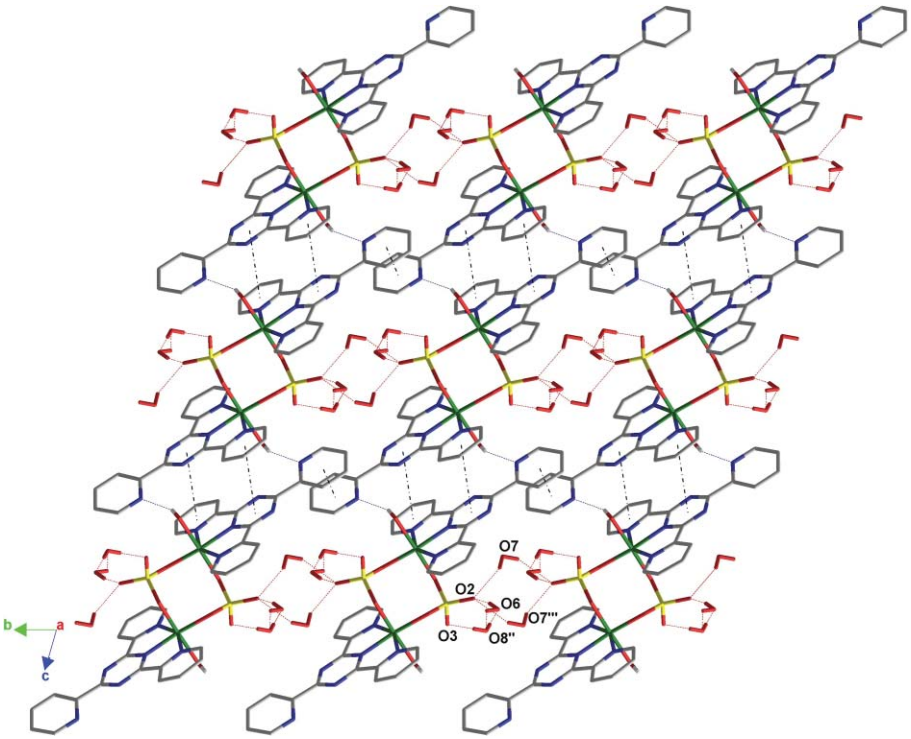

Fig. 9 Packing view of compound **8** showing π–π interactions within and between the ladders. Hydrogen atoms not involved in the interactions shown have been omitted for clarity reasons; water molecules have been evidenced using the red colour. Symmetry codes: ′ –x, –y, 1 – z; ″ 1 + x, y, z; ‴ –x, –1 – y, 2 – z.

H-bond involving the nitrogen atom and a hydrogen of the coordinated water molecule (O5-H5a · · · N2′: 2.02 Å, 2.794(7) Å, 153 °). The simultaneous presence in the nickel(II) coordination sphere of sulfate anions, water molecules, and aromatic (tptz) ligands leads to a nicely assembled packing where hydrophobic and hydrophilic forces work in concert. The dimeric units are connected with each other in three dimensions by means of π–π interactions between adjacent tptz units: along axis *c* the dimers are stacked in ladders piled through interactions involving the triazine and the $C_5N(4)$ pyridine rings [angle between planes: 1.66°, intercentroid distance: 3.65 Å]; the terminal $C_5N(6)$ pyridine rings are protruded out of the ladders along the *a* direction and interact with each other [0°, 3.54 Å] connecting the ladders (Fig. 9). Interactions between the $C_5N(4)$ and $C_5N(5)$ pyridine rings of adjacent ladders extend the network of aromatic interactions into the *b* direction (Fig. S6 in ESI†). Clustered in the hydrophilic areas, and ringed all around the sulfate groups, the solvent water molecules cement the molecular packing through numerous

hydrogen-bonding interactions mainly involving the sulfate anions (Fig. 9).

Conclusions

The reactivity between tptz and the differently substituted dithiophosphonato and dithiophosphato Ni^{II} complexes [Ni(ROpdt)$_2$] [ROpdt = (4-MeOPh)(RO)PS_2, R = Et (**2**), Pr (**3**), *i*-Pr (**4**), Bu (**5**),] and [Ni((EtO)$_2PS_2$)$_2$] (**6**) has been explored and the obtained neutral mixed complexes (**2**·tptz)–(**6**·tptz) have been characterised by means of single crystal X-ray diffraction. In all cases the incoming of one tptz molecule acting as tridentate ligand in the Ni^{II} coordination sphere detaches one of the sulfur atoms previously coordinated to the metal forcing one of the two dithiophosphonato/dithiophosphato ligands to behave as monodentate ligand. The presence of the monodentate dithiophosphonato/dithiophosphato ligands introduces a notable asymmetry in the Ni–S bond distances within isologous bidentate fragments, not found in similar Ni^{II} complexes. This asymmetry has been explained in terms of structural *trans*-effect (STE), as supported by DFT calculations. In our opinion, the lengthening of the *trans*-disposed Ni–S bonds might be responsible for the peculiar reactivity of the mixed complexes that easily undergo to partial or total replacement of the dithiophosphonato ligands. As a confirmation, the reaction of **2**·tptz with $AgNO_3$ and $CuSO_4$ yielded the complex [Ni(EtOpdt)(tptz)(H_2O)]NO_3 (**7**), and the dimer [(Ni(tptz)(μ-SO_4)(H_2O)]$_2$·6H_2O (**8**), respectively. It is interesting to note that the coordination chemistry of tptz and the nickel(II) ion has been recently explored, but among the range of different nickel-tptz complexes isolated in different reaction conditions, not one can be compared with the unusual dimer **8**, engendered from the mixed dithiophosphonato/tptz complexes.

Experimental

Materials and methods

All the reagents and solvents were purchased from Aldrich or Lancaster, and used without further purification. Elemental analyses were performed with an EA1108 CHNS-O Fisons instrument. FT-Infrared spectra were recorded on a Thermo Nicolet 5700 spectrometer at room temperature using a flow of dried air. Middle IR spectra (resolution 4 cm^{-1}) were recorded as KBr pellets, with a KBr beam-splitter and KBr windows. FT-Raman spectra (resolution of 4 cm^{-1}) were recorded as KBr solid mixtures on a Bruker RFS100 FT-Raman spectrometer, fitted with an In–Ga–As detector (room temperature) operating with a Nd-YAG laser (excitation wavelength 1064 nm) with a 180° scattering geometry. The excitation power was modulated between 100 and 250 mW.

Syntheses

Trans-bis[*O*-alkyl-(4-methoxyphenyl)dithiophosphonato]Ni complexes {[Ni(ROpdt)$_2$]; R = Et (**2**), Pr (**3**), *i*-Pr (**4**), Bu (**5**)} were synthesised according to previously reported procedures.[2,3]

[Ni((EtO)$_2PS_2$)$_2$] (6). $NiCl_2$·6H_2O (0.238 g, 1.001 mmol) and P_2S_5 (0.222 g, 0.499 mmol) were dissolved in 50 mL of EtOH and heated at reflux for 1 hour. After cooling to room temperature most of the solvent was removed by rotary evaporation to give a dark purple solid, which was then recrystallised using 10 mL of a solution of 1 : 1 ratio of CH_2Cl_2 and EtOH to give long purple crystals. Yield 0.399 g, 0.930 mmol, 87%. Mp 105 °C. Elemental analysis found (calc. for $C_8H_{20}O_4P_2S_4Ni$): C, 22.00 (22.39); H, 4.68 (4.70); S, 29.67 (29.88). FT-IR (1700–50 cm^{-1}): 1432 s, 1173 vs, 1020 s, 796 vs, 654 vs, 532 m, 469 m, 433 m, 396 m, 369 m, 353 m, 351 m, 333 w, 326 w, 325 vw, 302 w, 279 w, 246 w, 225 vw, 179 w, 151 m, 120 vw, 107 w, 74 w cm^{-1}. FT-Raman (1700–50 cm^{-1}; relative intensities in parentheses related to the highest peak taken equal to 10.0): 1472 (0.5), 1452 (1.1), 1388 (0.6), 1104 (1.5), 1053 (0.8), 1005 (0.4), 824 (2.0), 781 (1.1), 635 (3.4), 547 (9.6), 402 (1.9), 345 (2.2), 332 (4.4), 304 (4.7), 242 (3.3), 159 (6.3), 95 (10.0) cm^{-1}.

[Ni(EtOpdt)$_2$tptz] (2·tptz). Tptz (15.0 mg; 0.0480 mmol) and **2** (26.6 mg; 0.0480 mmol) were heated in 30 mL of EtOH in an Ace pressure tube until complete dissolution. The product was obtained as deep green crystals by slow evaporation of the solution at room temperature. Mp 89 °C. Elemental analysis found (calc. for $C_{36}H_{36}O_4P_2S_4N_6Ni$·$C_2H_5OH$): C, 50.14 (50.06); H, 4.18 (4.64); N, 9.42 (9.22); S, 13.73 (14.07). Yield: 29.7 mg, 0.0326 mmol, 68%. FT-IR (1700–50 cm^{-1}): 1594 s, 1573 m, 1557 vs, 1532 vs, 1498 m, 1374 s, 1293 ms, 1253 vs, 1174 m, 1110 s, 1027 vs, 1011 ms, 953 ms, 904 m, 830 m, 801 m, 768 vs, 684 mw, 664 vs, 653 vs, 636 m, 621 vs, 548 ms, 536 s, 332 w, 319 vw, 310 mw, 239 ms, 218 ms, 185 m, 145 ms, 136 w, 114 m cm^{-1}. FT-Raman (1700–50 cm^{-1}; relative intensities in parentheses related to the highest peak taken equal to 10.0): 1600 (3.7), 1571 (3.7), 1486 (5.0), 1402 (2.5), 1100 (3.7), 1026 (7.5), 1010 (2.5), 802 (1.2), 663 (3.7), 545 (5.0), 94 (10.0) cm^{-1}.

[Ni(PrOpdt)$_2$tptz] (3·tptz). Tptz (16.0 mg; 0.0512 mmol) and **3** (29.8 mg; 0.0512 mmol) were heated in 20 mL of PrOH in an Ace pressure tube until complete dissolution. The product was obtained as deep green crystals by slow evaporation of the solution at room temperature. MP 113 °C (dec). Elemental analysis found (calc. for $C_{38}H_{40}O_4P_2S_4N_6Ni$): C, 51.38 (51.07); H, 4.80 (4.51); N, 9.35 (9.40); S, 14.09 (14.35). Yield: 26.8 mg, 0.030 mmol, 59%. FT-IR (1700–50 cm^{-1}): 1594 m, 1573 m, 1558 vs, 1533 vs, 1497 ms, 1390 m, 1373 s, 1293 m, 1250 s, 1177 m, 1112 s, 1010 s, 829 m, 801 m, 766 s, 683 mw, 664 s, 640 s, 623 s, 547 m, 522 mw, 419 w, 352 m, 316 ms, 279 w, 253 w, 181 mw, 153 mw, 133 w, 106 mw, 87 mw cm^{-1}. FT-Raman (1700–50 cm^{-1}; relative intensities in parentheses related to the highest peak taken equal to 10.0): 1600 (5.2), 1570 (6.0), 1481 (7.6), 1398 (4.8), 1044 (6.2), 1011 (6.5), 549 (3.0), 90 (10.0) cm^{-1}.

[Ni(*i*-PrOpdt)$_2$tptz] (4·tptz). Tptz (15.5 mg; 0.0496 mmol) and **4** (28.9 mg; 0.0496 mmol) were heated in 30 mL of *i*–PrOH in an Ace pressure tube until complete dissolution. The product was obtained as deep green crystals by slow evaporation of the solution at room temperature. Mp 113 °C. Elemental analysis found (calc. for $C_{38}H_{40}O_4P_2S_4N_6Ni$): C, 51.23 (51.07); H, 4.80 (4.51); N, 9.39 (9.40); S, 14.09 (14.35). Yield: 23.8 mg, 0.0266 mmol, 54%. FT-IR (1700–50 cm^{-1}): 1594 m, 1575 ms, 1559 s, 1536 vs, 1497 m, 1394 m, 1375 s, 1293 s, 1257 s, 1247 s, 1175 ms, 1105 ms, 1026 m, 1011 m, 968 vs, 952 s, 877 m, 827 m, 800 m, 771 s, 753 s, 683 mw, 664 s, 646 m, 623 s, 559 s, 550 s, 399 s, 343 m, 293 m, 268 m, 185 s, 161 m, 146 w, 129 m, 104 ms cm^{-1}. FT-Raman (1700–50 cm^{-1}; relative intensities in parentheses related to the highest peak taken equal to 10.0): 1601 (5.0), 1570 (6.7), 1482 (8.3), 1401 (5.0), 1042 (6.7), 1028 (6.7), 1009 (5.0), 549 (3.3), 85 (10.0) cm^{-1}.

[Ni(BuOpdt)$_2$tptz] (5·tptz). Tptz (15.6 mg; 0.050 mmol) and **5** (26.8 mg; 0.050 mmol) were heated in 30 mL of BuOH in an Ace pressure tube until complete dissolution. The product was obtained as deep green crystals by slow evaporation of the solution at room temperature. Mp 86 °C. Elemental analysis found (calc. for $C_{40}H_{44}O_4P_2S_4N_6Ni$): C, 52.36 (52.13); H, 5.01 (4.81); N, 8.94 (9.12); S, 13.64 (13.91). Yield: 26.0 mg, 0.0282 mmol, 56%. FT-IR (1700–350 cm^{-1}): 1594 vs, 1575 vs, 1558 vs, 1536 vs, 1497 s, 1465 ms, 1450 ms, 1403 m, 1392 ms, 1375 vs, 1300 m, 1290 ms, 1255 ms, 1177 ms, 1110 s, 1059 ms, 1021 s, 1012 s, 999 ms, 970 s, 830 m, 800 ms, 770 vs, 683 m, 670 s, 649 ms, 637 s, 623 s, 565 m, 552 ms cm^{-1}. FT-Raman (1700–50 cm^{-1}; relative intensities in parentheses related to the highest peak taken equal to 10.0): 1583 (8.9), 1484 (10.0), 1438 (4.0), 1402 (7.0), 1373 (3.4), 1255 (1.5), 1182 (1.5), 1110 (2.6), 1046 (5.1), 1029 (9.4), 1010 (4.0), 993 (2.8), 802 (1.3), 635 (1.3), 83 (8.5) cm^{-1}.

[Ni((EtO)$_2$PS$_2$)$_2$tptz] (6·tptz). Tptz (0.15 g; 0.48 mmol) and **6** (0.21 g; 0.49 mmol) were heated in 30 mL of EtOH in an Ace pressure tube until complete dissolution in 50 mL of EtOH. The product was obtained as deep green crystals by slow evaporation of the solution at room temperature. Yield 0.236 g, 0.32 mmol, 67%. Mp 198 °C. Elemental analysis found (calc. for $C_{26}H_{32}N_6NiO_4P_2S_4$): C, 42.00 (42.12); H, 4.39 (4.35); N, 11.21 (11.33) S, 16.87 (17.30). FT-IR (1700–50 cm^{-1}): 1608 m, 1577 s, 1559 s, 1537 vs, 1486 m, 1473 m, 1443 m, 1395 ms, 1377 vs, 1258 mw, 1156 mw, 1098 m, 1042 s, 1011 vs, 947 s, 930 s, 774 vs, 684 ms, 658 vs, 635 ms, 551 m, 472 mw, 419 mw, 376 m cm^{-1}. FT-Raman (1700–50 cm^{-1}; relative intensities in parentheses related to the highest peak taken equal to 10.0): 1608 (4.6), 1586 (6.9), 1575 (8.4), 1484 (10.0), 1442 (3.5), 1402 (5.7), 1377 (3.0), 1260 (1.2), 1185 (1.3), 1046 (4.5), 1030 (8.4), 1010 (5.9), 994 (2.1), 815 (1.0), 780 (1.4), 706 (0.9), 664 (1.1), 634 (2.4), 553 (2.1), 492 (1.0), 374 (0.7), 334 (0.8) cm^{-1}.

[Ni(EtOpdt)(tptz)(H$_2$O)]NO$_3$ (7). A CH_3CN solution of $AgNO_3$ (5.0 mL; 7.0 mg; 0.04 mmol) was layered on a CH_2Cl_2 solution of **2**·tptz (5.0 mL; 34.6 mg; 0.04 mmol) in a dark tube, and stored in the darkness. After five weeks few deep ruby crystals have been isolated from a light brown solution. Due to the paucity of the product, only X-ray crystal structure and FT-IR analyses have been performed. FT-IR (4000–400 cm^{-1}): 3447 ms(br), 2982 m, 1653 w, 1589 ms, 1559 m, 1541 mw, 1497 ms, 1458 m, 1437 mw, 1386 mw, 1291 ms, 1254 s, 1181 ms, 1107 vs, 1016 s, 947 ms, 833 m, 800 mw, 773 mw, 658 ms, 633 ms, 621 s, 547 s, 517 m, 421 mw cm^{-1}.

[Ni(tptz)(μ-SO$_4$)(H$_2$O)]$_2$·6H$_2$O (8). A MeOH solution of $CuSO_4·5H_2O$ (5.0 mL; 5.0 mg; 0.02 mmol) was added to a CH_2Cl_2 solution of **2**·tptz (5.0 mL; 18.0 mg; 0.02 mmol) in a dark tube. The resulting yellow opaque solution was filtered and diethyl ether diffused on it. After three months few small green cubic crystals have been isolated. Due to the paucity of the product, only X-ray crystal structure and FT-IR analyses have been performed. FT-IR (4000–400 cm^{-1}): 3404 s(br), 1637 w, 1611 w, 1576 s, 1560 vs, 1542 vs, 1490 ms, 1477 ms, 1395 s, 1381 s, 1261 m, 1112 vs, 1048 s, 1032 ms, 860 m, 770 s, 740 w, 685 ms, 667 ms, 618 s, 490 m, 417 mw, 374 ms cm^{-1}.

X-Ray diffraction

X-Ray structure determinations and crystallographic data were collected at 293(2) K for compound **2**·tptz, and at 120(2) K for compounds **4**·tptz, **3**·tptz, **5**·tptz, **6**·tptz, **7**, and **8**, by means of combined phi and omega scans on a Bruker-Nonius KappaCCD area detector, situated at the window of a rotating anode (graphite Mo-K_α radiation for **4**·tptz, **3**·tptz, **6**·tptz, and 10 cm confocal mirrors for **5**·tptz, **7**, and **8**, respectively, $\lambda = 0.71073$ Å). The structures were solved by direct methods, SHELXS-97 and refined on F^2 using SHELXL-97.[22] Anisotropic displacement parameters were assigned to all non-hydrogen atoms. Hydrogen atoms were included in the refinement, but thermal parameters and geometry were constrained to ride on the atom to which they are bonded. The data were corrected for absorption effects using SORTAV[23] for **2**·tptz, **4**·tptz, and using SADABS V2.10[24] for **3**·tptz, **5**·tptz, **6**·tptz, **7**, and **8**. The disorder in compounds **2**·tptz, **5**·tptz, and **8** was modeled by splitting the respective residues of the molecules into two parts allowing the populations of the two sites to refine freely. In structure **5**·tptz the geometries of the disordered parts of the molecule had to be restrained to be the same for the two positions and rigid-body constraints were also applied.

Theoretical calculations

Quantum-chemical DFT calculations were carried out on compounds **2**·tptz and **6**·tptz with the mPW1PW[25] hybrid functional and Schafer, Horn, and Ahlrichs double-zeta plus polarization all-electron BSs[26] using the commercially available suite of programs Gaussian03.[27] NBO populations[28] and Wiberg bond indexes[29] were calculated at the geometries obtained from structural data.[30] The programs Gabedit 2.0.7[31] and Molden 4.6[32] were used to investigate the charge distributions and molecular orbital shapes.

Acknowledgements

CINECA (Consorzio Interuniversitario per il Calcolo Automatico dell'Italia Nord Orientale) is gratefully acknowledged.

References

1 A.-L. Cheng, N. L. Yan-Feng Yue, Y.-W. Jiang, E.-Q. Gao, C.-H. Yan and M.-Y. He, *Chem. Commun.*, 2007, 407–409; K. Biradha, M. Sarkar and L. Rajput, *Chem. Commun.*, 2006, 4169–4179; I. Goldberg, *Chem. Commun.*, 2005, 1243–1254; D. Braga, L. Brammer and N. R. Champness, *CrystEngComm*, 2005, **7**(1), 1–19; L. Brammer, *Chem. Soc. Rev.*, 2004, **33**, 476–489; S. Kitagawa, R. Kitaura and S.-I. Noro, *Angew. Chem. Int. Ed.*, 2004, **43**, 2334–2375; C. B. Aakeröy, J. Desper and J. Valdés-Martínez, *CrystEngComm*, 2004, **6**, 413–418; B. Rather and M. J. Zaworotko, *Chem. Commun.*, 2003, 830–831; N. L. Rosi, M. Eddaoudi, J. Kim, M. O'Keeffe and O. M. Yaghi, *CrystEngComm*, 2002, **4**, 401–404; F. A. Cotton, C. Lin and C. A. Murillo, *J. Chem. Soc. Dalton Trans.*, 2001, 499–501.
2 M. Arca, A. Cornia, F. A. Devillanova, A. C. Fabretti, F. Isaia, V. Lippolis and G. Verani, *Inorg. Chim. Acta*, 1997, **262**, 81–84.
3 M. C. Aragoni, M. Arca, F. Demartin, F. A. Devillanova, C. Graiff, F. Isaia, V. Lippolis, A. Tiripicchio and G. Verani, *J. Chem. Soc., Dalton Trans.*, 2001, 2671–2677.
4 I. Haiduc, *Handbook of Chalcogen Chemistry*, F. A. Devillanova, Ed., Royal Society of Chemistry, 2006, 593–643.
5 M. C. Aragoni, M. Arca, N. R. Champness, A. V. Chernikov, F. A. Devillanova, F. Isaia, V. Lippolis, N. S. Oxtoby, G. Verani, S. Z. Vatsadze and C. Wilson, *Eur. J. Inorg. Chem.*, 2004, **10**, 2008–2012.

6 M. C. Aragoni, M. Arca, N. R. Champness, M. De Pasquale, F. A. Devillanova, F. Isaia, V. Lippolis, N. S. Oxtoby, G. Verani and C. Wilson, *CrystEngComm*, 2005, **7**(60), 363–369.
7 M. C. Aragoni, M. Arca, F. A. Devillanova, M. B. Hursthouse, S. L. Huth, F. Isaia, V. Lippolis, A. Mancini, S. Soddu and G. Verani, *Dalton Trans.*, 2007, **21**, 2127–2134.
8 N. S. Oxtoby, A. J. Blake, N. R. Champness and C. Wilson, *Dalton Trans.*, 2003, 3838–3839.
9 X.-P. Zhou, X. Zhang, S.-H. Lin and D. Li, *Cryst. Growth Des.*, 2007, **7**, 485–487; X.-P. Zhou, D. Li, T. Wu and X. Zhang, *Dalton Trans.*, 2006, 2435–2443; X.-P. Zhou, D. Li, S.-L. Zheng, X. Zhang and T. Wu, *Inorg.Chem.*, 2006, **45**, 7119–7125; T. Glaser, T. Lugger and R. Frohlich, *Eur. J. Inorg. Chem.*, 2004, 394–400; N. Gupta, N. Grover, A. Neyhart, P. Singh and H. H. Thorp, *Inorg. Chem.*, 1993, **32**, 310–316.
10 Due to different reasons, commented in the cif files, the completeness for the structures of compounds **3**·tptz, **4**·tptz, **7**, and **8** is rather poor, and the overall data are not very good (high R_{int} values). However, the connectivity of the compounds could be established unambiguously. The resulting bond lengths are consistent with each other and with those here reported for analogous complexes, and have been considered in the following discussion.
11 Mogul 1.1.2, CSD 2008 release.
12 The data refer to 34 PS_2Ni fragments belonging to 29 different compounds (20 square-planar and 9 octahedral complexes), and were retrieved from the CSD using CCDC software (2008, v. 5.29). Oxidation states and coordination geometries were checked and ambiguous cases eliminated.
13 Originally, the term "*trans*-effect" was used to describe kinetic phenomena, whilst the term "*trans*-influence" was used to describe structural and thermodynamic phenomena. Following the recent review by B. J. Coe, and S. J. Glenwright, we'll adopt here the "expressions 'structural *trans*-effect' (STE) to refer to the effect of a ligand on the bond distance to a *trans* ligand and 'kinetic *trans*-effect' (KTE) to describe the effect on the lability of a *trans* ligand."B. J. Coe and S. J. Glenwright, *Coord. Chem. Rev.*, 2000, **203**, 5–80.
14 I. Haiduc and D. B. Sowerby, *Polyhedron*, 1996, **15**, 2469–2521; I. Haiduc, D. B. Sowerby and S.-F. Lu, *Polyhedron*, 1995, **14**, 3389–3472.
15 Data were retrieved from the CSD using CCDC software (2008, v. 5.29). Oxidation states and coordination geometries were checked and ambiguous cases eliminated: the reported data refer to 141 PS_2Ni fragments belonging to 105 different compounds {29 dithiophosphonato $[(R(RO)PS_2)^-]$, 58 dithiophosphato $[((RO)_2PS_2)^-]$, and 18 dithiophosphito $[(R_2PS_2)^-]$ complexes}.
16 A. A. Grinberg, *Izv. Inst. Izucheniyu Platiny*, 1932, **10**, 58.
17 J. K. Burdett and T. A. Albright, *Inorg. Chem.*, 1979, **18**, 2112.
18 K. M. Anderson and A. G. Orpen, *Chem. Commun.*, 2001, 2682–2683.
19 Search in the CSD (2008, v. 5.29) gave a mean value of 2.072 Å for 274 structures (628 fragments) with $R < 0.05$.
20 M. E. D. de Vivar, S. Baggio and R. Baggio, *Acta Crystallogr. Sect.E*, 2006, **62**, m986-m988; E. Freire, S. Baggio, J. C. Munoz and R. Baggio, *Acta Crystallogr. Sect. C*, 2002, **58**, m221-m224; P. Byers, G. Y. S. Chan, M. G. B. Drew and M. J. Hudson, *Polyhedron*, 1996, **15**(17), 2845–2849; G. A. Barclay, R. S. Vagg and E. C. Watton, *Acta Crystallogr. Sect. B*, 1977, **33**, 3487–3491.
21 R. Zibaseresht and R. M. Hartshorn, *Aust. J. Chem.*, 2005, **58**, 345–353.
22 G. M. Sheldrick, *SHELX suite of programs for crystal structure solution and refinement*, Univ. of Göttingen, Germany, 1997.
23 R. H. Blessing, *J. Appl. Cryst.*, 1997, **30**, 421–426.
24 G. M. Sheldrick, *SADABS, V2.10*, 2003.
25 C. Adamo and V. Barone, *J. Chem. Phys.*, 1998, **108**, 664.
26 A. Schafer, H. Horn and R. Ahlrichs, *J. Chem. Phys.*, 1992, **97**, 2571.
27 *Gaussian 03*, M. J. Frisch, G. W. Trucks, H. B. Schlegel, G. E. Scuseria, M. A. Robb, J. R. Cheeseman, J. A. Montgomery, Jr., T. Vreven, K. N. Kudin, J. C. Burant, J. M. Millam, S. S. Iyengar, J. Tomasi, V. Barone, B. Mennucci, M. Cossi, G. Scalmani, N. Rega, G. A. Petersson, H. Nakatsuji, M. Hada, M. Ehara, K. Toyota, R. Fukuda, J. Hasegawa, M. Ishida, T. Nakajima, Y. Honda, O. Kitao, H. Nakai, M. Klene, X. Li, J. E. Knox, H. P. Hratchian, J. B. Cross, V. Bakken, C. Adamo, J. Jaramillo, R. Gomperts, R. E. Stratmann, O. Yazyev, A. J. Austin, R. Cammi, C. Pomelli, J. W. Ochterski, P. Y. Ayala, K. Morokuma, G. A. Voth, P. Salvador, J. J. Dannenberg, V. G. Zakrzewski, S. Dapprich, A. D. Daniels, M. C. Strain, O. Farkas, D. K. Malick, A. D. Rabuck, K. Raghavachari, J. B. Foresman, J. V. Ortiz, Q. Cui, A. G. Baboul, S. Clifford, J. Cioslowski, B. B. Stefanov, G. Liu, A. Liashenko, P. Piskorz, I. Komaromi, R. L. Martin, D. J. Fox, T. Keith, M. A. Al-Laham, C. Y. Peng, A. Nanayakkara, M. Challacombe, W. P. M. Gill, B. Johnson, W. Chen, M. W. Wong, C. Gonzalez and J. A. Pople, Gaussian, Inc., Wallingford CT, 2004.
28 (*a*) A. E. Reed and F. Weinhold, *J. Chem. Phys.*, 1983, **78**, 4066; (*b*) A. E. Reed, R. B. Weinstock and F. Weinhold, *J. Chem. Phys.*, 1985, **83**, 735; (*c*) A. E. Reed, L. A. Curtiss and F. Weinhold, *Chem. Rev.*, 1988, **88**, 899.
29 K. Wiberg, *Tetrahedron*, 1968, **24**, 1083.
30 NBO Version 3.1, E. D. Glendening, A. E. Reed, J. E. Carpenter and F. Weinhold.
31 Gabedit is a free Graphical User Interface for computational chemistry packages. It is written by Abdul-Rahman Allouche. Gabedit is available from http://lasim.univ-lyon1.fr/allouche/gabeditb.
32 G. Schaftenaar and J. H. Noordik, *J. Comput.-Aided Mol. Design*, 2000, **14**, 123.

